

Bifurcation phenomena in a bi-directional coupled neural mass model

Hao Zhang(张浩), Lu Zhang(张路), Xiaoli Li(李小俚), Xiaonan Guo(郭肖楠), Dong Cui(崔冬)
Citation: Chin. Phys. B. 35, 098701 (2026). DOI: 10.1088/1674-1056/ae1df0 |
CSTR: 32038.14.CPB.ae1df0
http://cpb.iphy.ac.cn; http://iopscience.iop.org/cpb

What follows is a list of articles you may be interested in

Early identification of subjective cognitive decline using 2D horizontal visibility graph analysis of structural MRI networks

Huang-Jing Ni(倪黄晶), Yu-Fei Dai(戴雨菲), Ye Wu(吴烨), Jiao-Long Qin(秦姣龙), for the Alzheimer's Disease Neuroimaging Initiative (ADNI)
Chin. Phys. B. 35, 088701 (2026). DOI: 10.1088/1674-1056/ae2670 | CSTR: 32038.14.CPB.ae2670

Spiking activity in a meminductive and memristive emulator-based bionic circuit

Chenyu Zhang(张晨宇), Weiwei Fan(范伟伟), Huagan Wu(武花干), Ning Wang(王宁), Mo Chen(陈墨), Yibing Wang(王一冰), Quan Xu(徐权)
Chin. Phys. B. 35, 068707 (2026). DOI: 10.1088/1674-1056/ae4c72 | CSTR: 32038.14.CPB.ae4c72

Bursting synchronization induced by time-delay excitatory or inhibitory autapse in a minimal neuron–astrocyte network

Liao Yu(余廖), Wenlong Zhu(朱文龙), Zhuoqin Yang(杨卓琴), Zehan Luo(罗泽翰)
Chin. Phys. B. 35, 068705 (2026). DOI: 10.1088/1674-1056/ae48c2 | CSTR: 32038.14.CPB.ae48c2

Anti-interference ability of spiking neuron-astrocyte networks in working memory

Lin Li(李琳), Bingyi Mo(莫冰毅), Shanshan Cheng(程姗姗), Zhouchao Wei(魏周超), Ming Yi(易鸣), Lulu Lu(鹿露露)
Chin. Phys. B. 35, 068703 (2026). DOI: 10.1088/1674-1056/ae4e8c | CSTR: 32038.14.CPB.ae4e8c

Coupling-diversity-enhanced weak signal propagation in bistable networks

Yashi Zhang(章雅诗), Shanshan Cheng(程姗姗), Jie Fu(扶杰), Lulu Lu(鹿露露)
Chin. Phys. B. 35, 048704 (2026). DOI: 10.1088/1674-1056/ae23a9 | CSTR: 32038.14.CPB.ae23a9

Bifurcation phenomena in a bi-directional coupled neural mass model

Hao Zhang(张浩)[1,2], Lu Zhang(张路)[1,2], Xiaoli Li(李小俚)[3,4], Xiaonan Guo(郭肖楠)[1,2], and Dong Cui(崔冬)[1,2,†]

[1] *School of Information Science and Engineering, Yanshan University, Qinhuangdao* 066004, *China*
[2] *Hebei Key Laboratory of Information Transmission and Signal Processing, Yanshan University, Qinhuangdao* 066004, *China*
[3] *Guangdong Artificial Intelligence and Digital Economy Laboratory (Guangzhou), Guangzhou* 510335, *China*
[4] *School of Automation Science and Engineering, South China University of Technology, Guangzhou* 510641, *China*

(Received 9 October 2025; revised manuscript received 27 October 2025; accepted manuscript online 11 November 2025)

Electroencephalography (EEG) is a nonlinear dynamic complex chaotic signal. However, bifurcation analysis has been widely used as a nonlinear dynamics analysis method to explore EEG activity. We constructed a zero-delay bi-directional coupled Wendling neural mass model (BCWNMM) to simulate the functional brain network. Bifurcation analysis of the model was performed by changing the coupling strength and coupling direction to study the dynamic characteristics of the model. Finally, we used BCWNMM to simulate the EEG of epilepsy patients. Simulation results showed that when the model undergoes bidirectional coupling, various limit cycle oscillations (LCO) and bifurcation phenomena occur as the coupling coefficient changes. In addition, BCWNMM can generate epileptic-like EEG signals by adjusting the coupling strength. When the model undergoes unidirectional coupling, changes in the coupling strength cause the Wendling model of the emitting region to converge to different steady states, thereby triggering different bifurcation phenomena in the Wendling model of the receiving region. Our research results indicated that BCWNMM can generate EEG-like signals with rich dynamic characteristics, which can serve as a new method for studying the connection between two brain regions.

Keywords: electroencephalography, bi-directional coupled Wendling neural mass model, bifurcation analysis, epilepsy

PACS: 87.19.le, 47.20.Ky, 87.85.Ng, 87.19.xm

DOI: 10.1088/1674-1056/ae1df0 **CSTR:** 32038.14.CPB.ae1df0

1. Introduction

The brain is an unstable, nonlinear, complex dynamical system.[1] An electroencephalogram (EEG) is a representation of the overall synaptic potential generated by interactions between neurons.[2] With the development of neuroscience, researchers hope to use mathematical modeling to simulate the process by which neuronal activity generates EEG, thereby exploring the mechanisms of brain rhythms and the pathogenesis of brain diseases such as epilepsy and Alzheimer's disease.[3,4]

In recent years, the neural mass model (NMM) has become a popular tool for investigating nonlinear neural connections in the brain.[5,6] The NMM is a lumped parameter model used to simulate groups of neurons with similar discharge characteristics at the mesoscopic level.[7] Therefore, the NMM can reflect the average discharge behavior of neuronal populations in the brain. The concept of NMM was first proposed by Freeman,[8] and subsequently López da Silveira *et al.*[9] proposed a lumped parameter model capable of generating alpha rhythms. Jansen and Rit *et al.*[10] proposed the Jansen & Rit neural mass model for simulating EEG signals. The Jansen & Rit neural mass model can generate EEG-like signals and visual arousal potentials, and includes pyramidal neurons, excitatory interneurons, and inhibitory interneurons. Wendling *et al.*[11] added a fast inhibitory loop to the Jansen & Rit neural mass model, enabling the model to generate gamma rhythm signals.

Since the brain processes and integrates information through the interconnection of neuronal populations, single-region NMM may not reflect complex behaviors such as information exchange between neuronal populations. Therefore, researchers also tended to construct more complex NMM to mathematically model brain electrophysiological activity. David and Friston[12] constructed a dual-dynamic, dual-channel coupled NMM to analyze the effects of excitatory and inhibitory parameters on signal frequency. Cui *et al.*[13] established a multi-dynamic, multi-channel brain region coupling model to explore the working mechanisms of brain networks at the macro level. Han *et al.*[14] constructed a Whole-brain network model (WBNM) consisting of 78 nodes to study strategies for intervening in neuronal excitability levels and methods for delaying the decline in brain functional connectivity. Honey *et al.*[15] constructed a high-resolution WBNM based on the Larter–Breakspear model[16,17] and studied the interrelationships between structural connectivity, functional connectivity, and cross-regional distance. The WBNM has evolved from a concept into a practical research method.[18] Since the

†Corresponding author. E-mail: cuidong@ysu.edu.cn

© 2026 Chinese Physical Society and IOP Publishing Ltd. All rights, including for text and data mining, AI training, and similar technologies, are reserved.

basic unit of WBNM is the coupling between two regions connected by NMM, it is necessary to study the coupling phenomenon between two regions connected by NMM.

Bifurcation analysis is a method for studying changes in system dynamics. It can be used to study the number and stability of equilibrium points in a system, the number and type of bifurcation points (BP), the stability of limit cycle oscillations (LCO), and folding phenomena, when one or more parameters change continuously.[19] The NMM is a nonlinear dynamical system described by a set of differential equations. Researchers can gain a deeper understanding of the mechanism by which the NMM generates signals by applying bifurcation theory to study the dynamical properties of the NMM.[20] Grimbert *et al.*[21] used bifurcation theory to analyze the monostable, bistable, and LCO characteristics of the single-region Jansen & Rit neural mass model when the external noise input changes continuously. Huang *et al.*[22] studied the bifurcation and chaos characteristics of two Jansen & Rit neural mass models using the maximum Lyapunov exponent and found that stable equilibrium points, limit cycles, and chaotic attractors can coexist under different connection parameters. Xin *et al.*[23] designed a Hamiltonian energy control system and used bifurcation theory to analyze the existence and stability of equilibrium points in two generalized Lorentz systems, proving that the hidden attractor coexists with the states of stabilization, period, chaos, and even transient chaos. Bazada *et al.*[24] investigated the relationship between alpha oscillation activity and bifurcation behavior and found that the inhibitory connection pathway from the thalamic reticular nucleus cell group to the thalamic cortical relay cell group played a key role in the weakening of alpha activity in the simulated model output. Said *et al.*[25] constructed a coupled NMM and drew a bifurcation diagram. They then correlated the model output results with epileptic signals and used the nonlinear dynamic characteristics of the coupled model to explain the causes of epileptic signals. Clusella *et al.*[26] simplified the whole-brain network model using the averaging method and revealed the lateral instability of whole-brain synchronization by analyzing the simplified model.

In our previous study, we used the Wendling model to construct WBNM.[27–29] However, we lacked understanding of the neural dynamics between different regions in WBNM. Due to the inherent temporal delays in information transmission between different brain regions,[30] to avoid the complex dynamic behaviors caused by these delays themselves and to focus more on studying the nonlinear relationships between neural ensemble models,[31] the present study has constructed a zero-delay bi-directional coupled Wendling neural mass model (BCWNMM). Subsequently, bifurcation analysis was employed to investigate the bifurcation phenomena arising from adjustments to the coupling strength and direction within the model. The stable equilibrium points, unstable equilibrium points, limit cycles, and other steady states of the BCWNMM were studied, as well as the effects of different steady states on the output results of the BCWNMM. We compared these with the nonlinear dynamical characteristics of the single-region model and revealed the existence of multiple bifurcation phenomena in the BCWNMM. Finally, we used BCWNMM to simulate EEG data from epilepsy patients. The findings of the study suggest that a sudden surge in the strength of coupling between disparate regions of the brain may serve as a potential causative factor for epileptic seizures.[32]

The structure of this experimental study is as follows: Subsection 2.2 introduces the BCWNMM; Subsection 3.1 performs symmetric bifurcation analysis on this model; Subsection 3.2 analyzes the steady-state phase diagram and bifurcation curve waveforms at bifurcation points; Subsection 3.3 investigates asymmetric bifurcation curves; Subsection 3.4 analyzes the unidirectional coupling branch of the BCWNMM. Finally, Subsection 3.5 utilizes the BCWNMM to simulate EEG characteristics during epileptic seizures.

2. Models and methods

2.1. Wendling neural mass model

Miles *et al.*[31] identified two types of transmitter gamma-aminobutyric acid (GABA) inhibitory synaptic responses in CA1 pyramidal neurons: GABAA-slow and GABAA-fast. Banks *et al.*[33] found that GABAA-slow interneurons not only inhibit pyramidal cells but also inhibit GABAA-fast interneurons. Therefore, Wendling *et al.*[11] added a fast inhibitory circuit to the Jansen & Rit neural mass model, which represents a group of fast inhibitory interneurons that can act simultaneously on pyramidal cells and inhibitory neurons. The structure of the Windelin model is shown in Fig. 1.

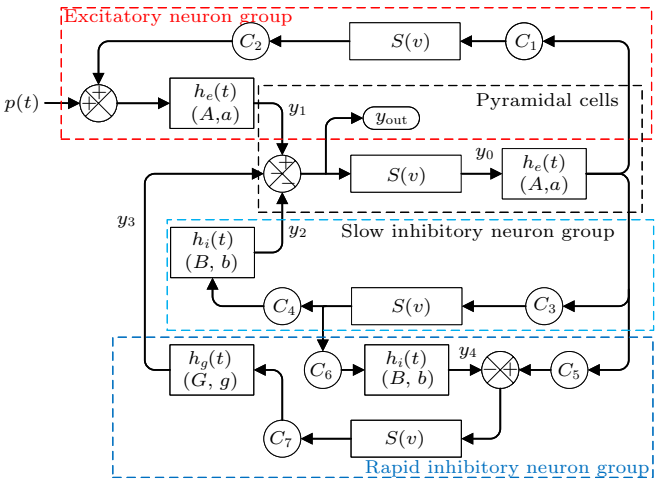


Fig. 1. The Wendling neural mass model structure diagram.

The Wendling model consists of four components: pyramidal cells, excitatory neurons, inhibitory neurons, and rapid

inhibitory neurons. The model simulates excitatory synapses from pyramidal cells to three types of interneurons and receives excitatory and inhibitory feedback from interneurons. C_1, C_2, C_3, and C_4 represent the synaptic connection constants of cell groups, C_5 and C_6 are the average synaptic connection parameters of rapid inhibitory feedback loops, and C_7 represents the average synaptic connection parameter between slow inhibitory neurons and rapid inhibitory neurons. $p(t)$ represents interference or external noise received by the cerebral cortex from neighboring regions. In this study, it is represented by Gaussian white noise with a mean of μ and a variance of σ^2.

Functions $h_e(t)$, $h_g(t)$, and $h_i(t)$ are linear dynamic transfer functions that convert the average pulse density of action potentials into excitatory and inhibitory postsynaptic membrane potentials, as shown below

$$h_e(t)=\begin{cases} Aat\,\mathrm{e}^{-at}, & t\geq 0,\\ 0,, & t<0,\end{cases}\quad h_i(t)=\begin{cases} Bbt\,\mathrm{e}^{-bt}, & t\geq 0,\\ 0, & t<0,\end{cases}$$
$$h_g(t)=\begin{cases} Ggt\,\mathrm{e}^{-gt}, & t\geq 0,\\ 0, & t<0,\end{cases} \tag{1}$$

where A is the excitatory gain, B represents the slow inhibitory gain, and G represents the fast inhibitory gain. Parameters A, B, and G affect the maximum amplitude of the postsynaptic membrane potential. a, b, and g represent the reciprocals of the average time constants for the excitatory process, slow inhibitory process, and fast inhibitory process, respectively. Parameters a, b, and c affect the position of the maximum amplitude. e denotes the natural index. The nonlinear static transfer function $S(v)$ converts the postsynaptic membrane potential into the average pulse density of action potentials. This process is typically implemented using a Sigmoid function

$$S(v)=\frac{2e_0}{1+\mathrm{e}^{r(v_0-v)}}, \tag{2}$$

where $2e_0$ is the maximum discharge rate of the neuron group. v_0 is the postsynaptic membrane potential when the discharge rate reaches e_0. r is the slope of the curve of function $S(v)$. The Wendling NMM can be expressed as the following differential equation

$$\begin{aligned}
&\dot{y}_0(t)=y_5(t),\\
&\dot{y}_1(t)=y_6(t),\\
&\dot{y}_2(t)=y_7(t),\\
&\dot{y}_3(t)=y_8(t),\\
&\dot{y}_4(t)=y_9(t),\\
&\dot{y}_5(t)=AaS\{y_1(t)-y_2(t)-y_3(t)\}-2ay_5(t)-a^2y_0(t),\\
&\dot{y}_6(t)=Aa\{p(t)+C_2S(C_1y_0(t))\}-2ay_6(t)-a^2y_1(t),\\
&\dot{y}_7(t)=Bb\{C_4S(C_3y_0(t))\}-2by_7(t)-b^2y_2(t),\\
&\dot{y}_8(t)=Gg\{C_7S(C_5y_0(t)-y_4(t))\}-2gy_8(t)-g^2y_3(t),\\
&\dot{y}_9(t)=Bb\{C_6S(C_3y_0(t))\}-2by_9(t)-b^2y_4(t),
\end{aligned} \tag{3}$$

where y_{out} is the model output, which is defined in the following expression:

$$y_{\mathrm{out}}=y_1-y_2-y_3. \tag{4}$$

2.2. Double Wending coupling model

We constructed a zero-delay BCWNMM to study the nonlinear dynamic characteristics of a bidirectional coupled NMM. As shown in Fig. 2, the output of model i is processed by the sigmoid function $S(v)$, multiplied by the coupling coefficient C, and superimposed with noise $P(t)$, and then used as the input of the model j. Similarly, the output of the model j undergoes the same processing and is used as the input of the model i.

The differential equation system of the BCWNMM is as follows:

$$\begin{aligned}
\dot{y}_0^i(t) &= y_5^i(t),\\
\dot{y}_1^i(t) &= y_6^i(t),\\
\dot{y}_2^i(t) &= y_7^i(t),\\
\dot{y}_3^i(t) &= y_8^i(t),\quad \dot{y}_4^i(t)=y_9^i(t),\\
\dot{y}_5^i(t) &= AaS\left[y_1^i(t)-y_2^i(t)-y_3^i(t)\right]-2ay_5^i(t)-a^2y_0^i(t),\\
\dot{y}_6^i(t) &= Aa\left\{p(t)+C\sum_j C_{ij}S\left[y^j(t)\right]+C_2S\left[C_1y_0^i(t)\right]\right\}\\
&\quad -2ay_6^i(t)-a^2y_1^i(t),\\
\dot{y}_7^i(t) &= BbC_4S\left[C_3y_0^i(t)\right]-2by_7^i(t)-b^2y_2^i(t),\\
\dot{y}_8^i(t) &= GgC_7S\left[C_5y_0^i(t)-y_4^i(t)\right]-2gy_8^i(t)-g^2y_3^i(t),\\
\dot{y}_9^i(t) &= BbC_6S\left[C_3y_0^i(t)\right]-2by_9^i(t)-b^2y_4^i(t),
\end{aligned} \tag{5}$$

where i and j are the serial numbers of different brain region channels, respectively. $C_{ij}S[y^j(t)]$ represents channel i receiving input signals from j. C_{ij} indicates the structural connection strength between channel i and channel j.[34]

Since we only studied the coupling between two channels, the coupling strength C and C_{ij} can be combined into one term, denoted as C.

Output Y_k is shown in the following equation:

$$Y_k=y_1^k(t)-y_2^k(t)-y_3^k(t),\quad k=i,j, \tag{6}$$

where k is the output channels. The standard parameters applied in the BCWNMM in the present research are shown in Appendix A.

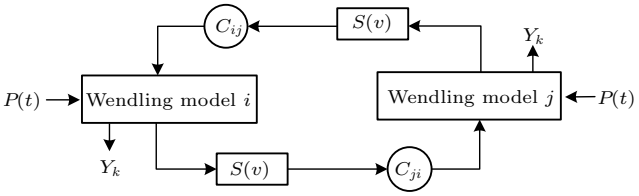


Fig. 2. The BCWNMM structure diagram.

2.3. Epilepsy data

The epilepsy experimental dataset contains EEG signals recorded from epilepsy patients during interictal and ictal periods, collected by Piyush *et al.*[35] at the Centre for Neurology and Sleep Disorders in New Delhi. The data acquisition system uses a Grass Telefactor Comet AS40 amplification system with a sampling frequency of 200 Hz and a frequency range of 0.5 Hz to 70 Hz. The dataset is divided into three phases: pre-seizure, interictal, and ictal, each lasting 5.12 seconds.

3. Result

Bifurcation diagrams can be used to illustrate the dynamic characteristics of different parameter systems in bifurcation analysis. We plotted a residual bifurcation diagram with constant C as the parameter to study the nonlinear dynamic characteristics under different coupling strengths and explore the generation mechanism of EEG signals in epilepsy patients.

3.1. Symmetric bifurcation diagram

We plotted the bifurcation diagram of the BCWNMM to study the dynamic characteristics of the BCWNMM when the coupling strength C changes. For the model parameters of channels i and j, refer to the parameter settings in Appendix A.

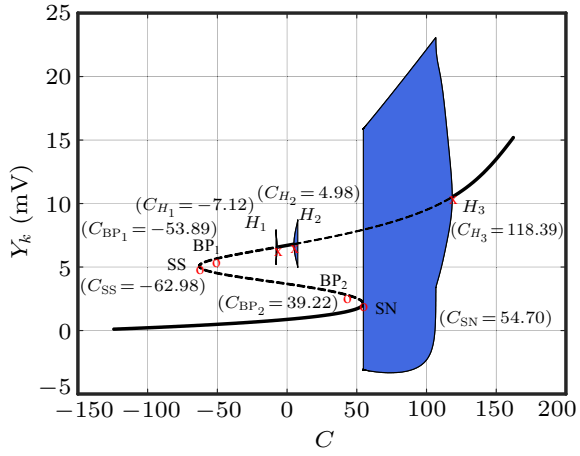


Fig. 3. Bifurcation diagram of C for BCWNMM.

Figure 3 shows the BCWNMM bifurcation curve as a function of C. Since model i and model j are symmetrical to each other, the output results of these two models are consistent. Solid lines indicate stable equilibrium points, while dashed lines indicate unstable equilibrium points. The bifurcation point in Fig. 3 is marked in red, and the limit cycle is marked in blue. A saddle–node point bifurcation (SN) is formed at point $C = 54.70$, and a saddle–saddle bifurcation (SS) is formed at point $C = -62.98$. These two bifurcation points form a multi-stable region and coexisting orbit rings. H_1, H_2, and H_3 are three supercritical Hopf bifurcation points formed at points $C = -7.12$, $C = 4.98$, and $C = 118.39$, respectively. Among them, the limit cycle generated by H_3 (blue area in the figure) disappears at SN, which is analogous to the limit cycle generated at the subcritical Hopf bifurcation point in the Jansen & Rit neural mass model.[36] The BCWNMM produced two types of bifurcation diagrams: symmetric and asymmetric. These diagrams resemble the results reported by Ahmadizadeh *et al.*[25] The model becomes more susceptible to the influence of the lower branch equilibrium point when $C < 54.7$. The model is simultaneously affected by both the H_3 bifurcation point and the SN bifurcation point when $C > 54.7$. This marks a transition from a stable to an unstable state in the model, potentially indicating a shift in brain state from resting to task-related activity. As the C value continues to rise and approaches the H_3 bifurcation point, the output exhibits sinusoidal characteristics. This may reveal the brain's transition process from a task-active state back to a resting state.

3.2. Steady-state phase diagram and waveform of symmetric bifurcation diagram

Figure 4 shows all steady-state phase diagrams and waveform outputs of the BCWNMM. Figure 4(a) shows the phase diagram and waveform diagram when the BCWNMM converges to the lower branch, and Fig. 4(b) shows the phase diagram and waveform diagram when the BCWNMM converges to the upper branch. Both of these steady states are stable equilibrium points, and as the number of iterations increases, the waveform output gradually tends toward a straight line. Figure 4(c) shows the phase diagram and waveform diagram of the H_1 bifurcation point, and Fig. 4(d) shows the phase diagram and waveform diagram of the H_2 bifurcation point. Both the H_1 and H_2 bifurcation points can produce stable limit cycle oscillations, and the limit cycles produced by both are close to circular. Furthermore, the waveforms at the H_1 and H_2 bifurcation points are harmonic oscillations, but the amplitude of the H_1 waveform is slightly higher than that of the H_2 waveform.

As shown in Figs. 4(e)–4(g), to observe the steady-state conditions of the limit cycle oscillations generated by the blue region in Fig. 3, we set the coupling strength to $C = 55$, $C = 90$, and $C = 100$, respectively, and plotted the phase diagram and waveform diagram of the limit cycle oscillations originating from H_3 and disappearing at SN. In addition, the shape of the limit cycle gradually tends toward a circle as the coupling strength C increases, the frequency of the generated waveform increases while the amplitude decreases, and the corresponding waveform gradually approaches a sine waveform. Figure 4(h) shows the phase diagram and output waveform when $C = 150$, where the BCWNMM converges to the equilibrium point marked with a red asterisk. The convergence results at this point are similar to those in Fig. 4(a).

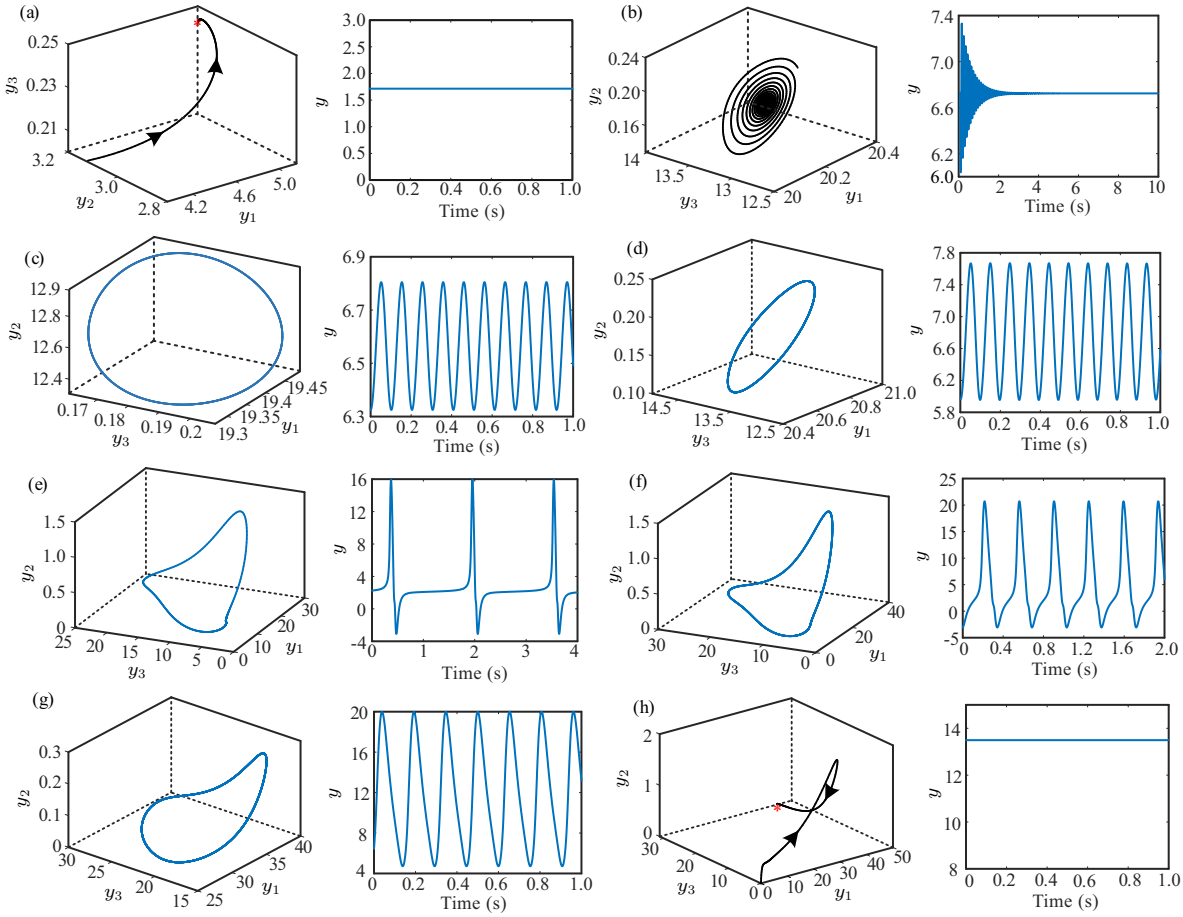


Fig. 4. Phase diagrams of BCWNMM.

In addition, we found that the phase diagram of the limit cycle oscillations generated at H_3 has multiple shapes. Therefore, we plotted the variation curves of the amplitude and main frequency when the limit cycle oscillations generated at H_3 continuously vary with the coupling strength C. The results are shown in Fig. 5. As shown in Fig. 5, the curve tends toward the limit cycle of different principal frequencies as the C value changes. As shown in Fig. 5(a), when $55 \leq C \leq 88$, the limit cycle in this range produces a spike-like signal. The main frequency of the waveform output by the BCWNMM initially approaches 3 Hz when $80 \leq C \leq 118.39$, then suddenly rises to 6 Hz, and finally continues to rise steadily as C changes. This indicates that limit cycles generated by the same supercritical Hopf bifurcation point can produce different types of waveforms, and even waveforms of the same type may have different fundamental frequencies and amplitudes.

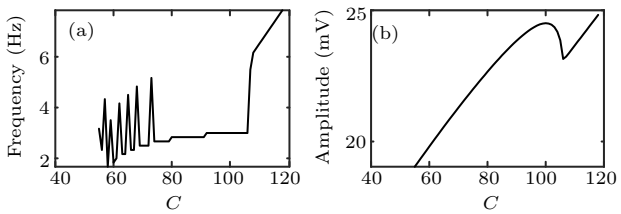


Fig. 5. The amplitude and dominant frequency of limit cycles generated by H_3.

3.3. Asymmetric bifurcation curve

Figure 6 shows the changes in the asymmetric bifurcation curve and steady state of BCWNMM at the bifurcation point as the C value varies. Figure 6(a) shows the asymmetric bifurcation curve generated at the BP_1 bifurcation point, where SN_1 and SN_2 are the saddle-node bifurcation points generated in this asymmetric bifurcation curve. Figure 6(b) shows the asymmetric bifurcation curve generated at the BP2 bifurcation point. In addition, BCWNMM has two asymmetric bifurcation curves, both of which originate from the BP bifurcation point. We used different colors to mark bifurcation curves with the same properties between two channels. Solid lines indicate stable equilibrium points, while dashed lines indicate unstable equilibrium points. When channel i converges to any point on the pink solid line, channel j will also converge to the corresponding position on the pink solid line, rather than any point on the blue curve.

As shown in Figs. 6(a) and 6(b), the dynamic characteristics of channels i and j are consistent but not synchronized. Furthermore, when the initial value C is the same, the two channels converge to different types of attractors. Therefore, the system exhibits bistable characteristics in this case of asymmetric bifurcation. As shown in Fig. 6(b), the equilibrium points on the bifurcation curve are all unstable equilib-

rium points in the asymmetric bifurcation diagram generated at point BP_2, so they do not affect the model output.

Figures 6(c) and 6(d) show the steady-state phase diagrams for channels i and j, respectively. The black dots represent any stable equilibrium points between H_1 and H_2 in Fig. 3, the blue limit cycles are limit cycles generated by the oscillations of the limit cycle at point H_3 in Fig. 3, and the yellow and pink star points represent any equilibrium points on the corresponding colored curves in Figs. 6(a) and 6(b). Figure 6(d) shows the output waveforms of these four steady states. Both symmetric bifurcation diagrams and asymmetric bifurcation diagrams affect the output of the coupled model. Therefore, changes in coupling strength C will affect the type and number of steady states in the system and cause the BCWNMM to produce multiple limit cycle oscillations. As shown in Fig. 3, H_1, H_2, and H_3 can all produce stable limit cycles, while the limit cycles produced by H_3 can generate waveforms with different fundamental frequencies and amplitudes, reflecting the complexity of the dynamic characteristics of the coupled model. Moreover, both symmetric and asymmetric bifurcation diagrams are subject to restrictions in the form of a set of equations. In addition, the steady state of both channels is affected by continuous changes in the coupling strength C. In asymmetric bifurcation diagrams, the model exhibits more complex dynamical properties, revealing additional bifurcation curves and steady states. At this point, the model is influenced by more steady states, leading to an increase in the number of convergence paths. This may indicate that when the brain operates at the critical boundary between resting and task states, its sensitivity to state transitions is heightened. As shown in Fig. 6(a), the C values corresponding to the SN_1 and SN_2 are identical; this noteworthy phenomenon indicates that the coupling critical thresholds for state transitions in the model are the same. This may suggest that when the brain approaches the critical state of a state transition, its coupling characteristics exhibit similarities.

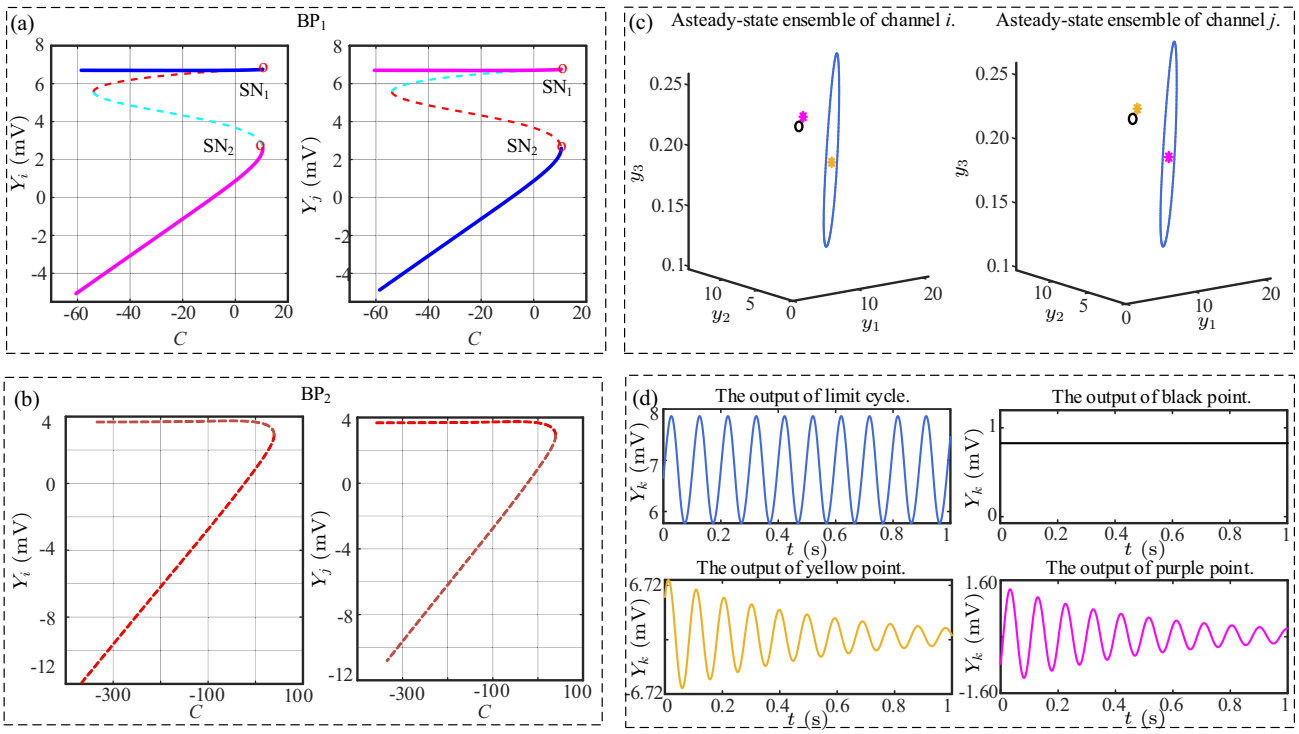


Fig. 6. Changes in the asymmetric bifurcation curve and steady-state conditions of BCWNMM at the bifurcation point as C varies: (a) the bifurcation situation of regions i and j at point BP_1; (b) the bifurcation situation of regions i and j at point BP_2; (c) the local steady-state phase diagram of regions i and j; (d) the output waveform of BCWNMM under steady-state conditions.

3.4. Unidirectional coupling branch analysis

In this section, we investigated the effect of coupling strength C on the steady state of the entire BCWNMM system under unidirectional coupling and compared it with the dynamic characteristics of the bidirectional coupling system. The output of channel i will be used as the input of channel j, but channel i will not receive the input of channel j when BCWNMM performs unidirectional coupling. Since channel i is not affected by the output signal of channel j, the dynamic characteristics of channel i are completely consistent with the Wendling model. Therefore, we studied the dynamic characteristics of channel j.

Figure 7 shows the bifurcation diagram of channel i, which is consistent with the results of Geng *et al.*[37] on the Wendling model. Figure 7(a) shows a subcritical Hopf bifurcation point H and a saddle-node bifurcation point SN. The yellow area indicates the unstable limit cycle generated by bifurcation point H. The red vertical line indicates external dis-

turbance ($P = 90$). The black solid line below point SN indicates the lower branch, and the black solid line above point H indicates the upper branch. Channel i has two steady states when $P = 90$. Therefore, we can change the initial values of the system so that channel i converges to different steady states and study the dynamic characteristics of channel j. Due to the bistable effect of channel i on the unidirectional coupling model, channel j has two bifurcation diagrams that converge to the upper and lower branches, respectively. The intersection of the upper branch line and the red vertical line in the phase diagram indicates that the output value approaches the equilibrium point (red asterisk) in an almost linear manner. The intersection of the lower branch line and the red vertical line in the phase diagram indicates that the output approaches the equilibrium point (red asterisk) in a spiral manner.

Therefore, the system has two steady states when it is coupled in a unidirectional manner. Figure 7(b) shows the branch graph of channel j when channel i converges to the lower branch and upper branch, respectively. When channel i converges to the lower branch, channel j has three bifurcation points (*i.e.*, H, SN, and SS), and the appearance of SS and SN gives the system a bistable characteristic, which is consistent with the research results in the bidirectional coupling model. Although the subcritical Hopf bifurcation point H can generate limit cycle oscillations, the limit cycle is unstable, and therefore the system cannot produce periodic oscillatory output. In addition, when channel i converges to the upper branch, channel j only has a stable equilibrium point and does not produce a stable limit cycle. The initial positions and ranges of action of the single-stable region and the double-stable region are different, with the double-stable region ($C \geq 0$) having a smaller range of action.

Figure 7(c) shows the phase diagram and output of channel j when channel i in Fig. 7(b) converges to the lower steady state and upper steady state, respectively, as well as the phase diagram and output of channel j when channel j converges to the upper steady state in the orange region in Fig. 7(b). The output of channel j is mainly affected by the convergence of channel i to the lower branch in the initial stage when channel i converges to the lower branch. Since the external input $P(t)$ follows a Gaussian white noise distribution with a specific mean and variance, channel i may converge to the upper branch under certain initial values. Therefore, this may cause channel j to converge to the bifurcation curve, where channel i converges to the upper branch in Fig. 7(b). The output of the coupled system is affected not only by the multi-stability of channel j, but also by the initial value in unidirectional coupling.

In addition, both bifurcation diagrams will affect the output for the entire coupled model. Furthermore, external noise $P(t)$ is mainly Gaussian white noise in most cases. Due to the variability of the $P(t)$ and the complexity of the model solution process, we can only determine which steady state the model will be affected by drawing a bifurcation diagram, but we cannot determine the specific moment when the model converges to the steady state.

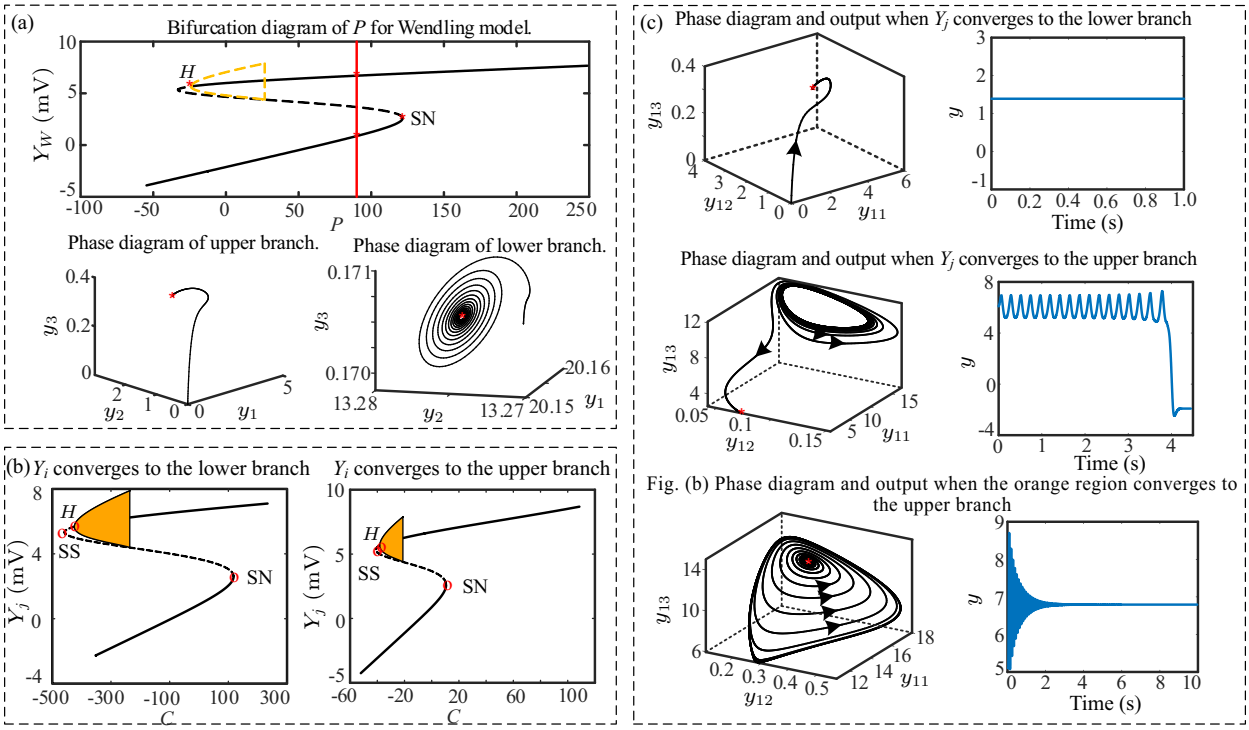


Fig. (b) Phase diagram and output when the orange region converges to the upper branch

Fig. 7. Results of unidirectional coupling bifurcation analysis: (a) the bifurcation diagram generated by the Wendling model when the input parameter $P(t)$ changes; (b) the bifurcation diagram of region j when region i converges to the upper and lower branches, respectively, where C is a variable; (c) the change in the phase diagram when channel j converges.

3.5. Research on epilepsy signals

Epilepsy is a brain disorder caused by abnormal electrical discharges in the brain's neurons.[38,39] The study simulates the generation of epileptic signals by changing the coupling coefficient C and explores the nonlinear dynamic characteristics of this model. Researchers can obtain EEG signals similar to those of epilepsy patients by adjusting parameters A, B, and G in NMM.[40] This study found that signals similar to those of epileptic patients' EEG signals can be generated by adjusting the global coupling strength C in the BCWNMM model. The parameter settings are detailed in Appendix A. The sampling frequency is 200 Hz. The time length is 1 s.

Figure 8 shows the epileptic EEG signals generated by the BCWNMM by changing the coupling coefficient C. Figure 8(a) shows the EEG signals of the patient during an epileptic seizure. Figure 8(b) shows the epileptic seizure-like EEG signals generated by BCWNMM, where $C = 30$. As shown in Figs. 8(a) and 8(b), the peak frequencies of both sets of EEG signals did not exceed 0.1, and the spectra were concentrated within 12 Hz. The frequency components of the two sets of signals were similar.

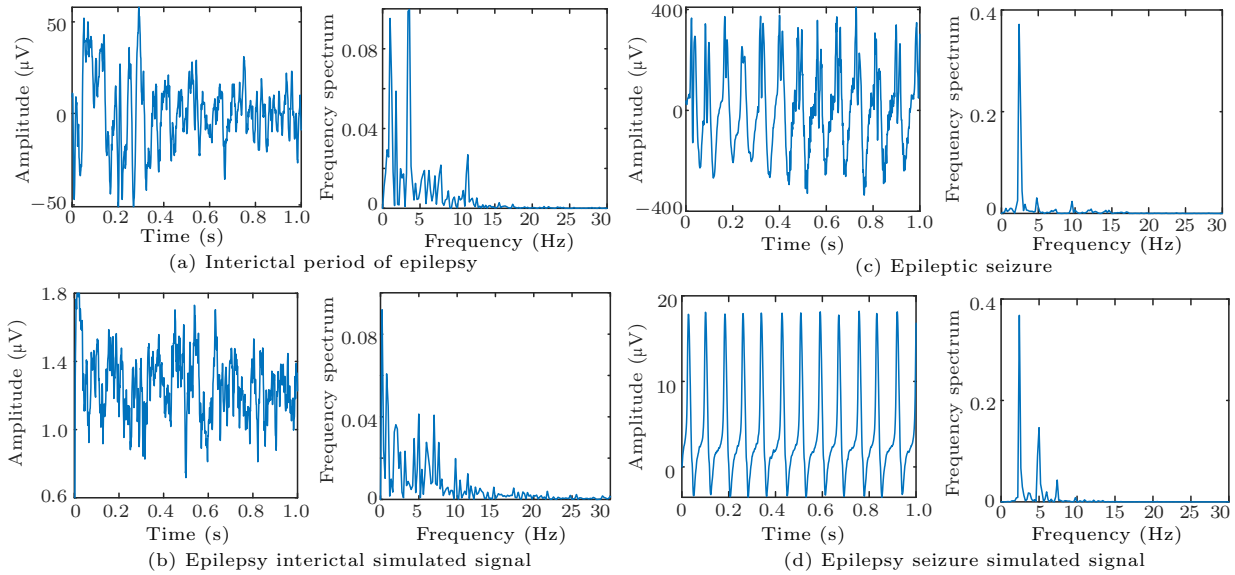


Fig. 8. The BCWNMM simulation of epileptic EEG signals: (a) interictal EEG signal; (b) interictal EEG signal generated by BCWNMM, $C = 30$; (c) epileptic seizure EEG signal; (d) epileptic seizure EEG signal generated by BCWBMM, $C = 70$.

Figure 8(c) shows the EEG signal of the patient during the interictal period. Figure 8(d) shows the brain-like EEG signal generated by BCWNMM during the interictal period, where $C = 70$. Since the waveforms of both signals are continuous spike signals, the main frequencies in the spectrum diagram are concentrated within 10 Hz, and the main peaks do not exceed 0.4. The frequency components of the two signals are similar. The results indicate that the BCWNMM can generate signals similar to epileptic EEG signals by adjusting the parameter C. Therefore, a sudden increase in the coupling strength between different brain regions may be one of the causes of epileptic seizures.[32]

4. Discussion

The NMM has rich nonlinear dynamic characteristics, and different dynamic characteristics lead to different types of model outputs. The application of bifurcation theory in the analysis of neural network models facilitates the exploration of the mechanisms underlying the generation of EEG signals by NMM. Regardless of whether the NMM is of the single-channel variety or the dual-channel coupled variety, a multitude of complex dynamic characteristics will manifest in conjunction with one another within a relatively limited range of parameters. The brain is a highly nonlinear system, meaning its activity state is dependent on its internal neural activity. State transitions manifest as continuous dynamic driving processes. It is widely acknowledged that common transitions include the following: the transition between the resting and task states; the transition between wakefulness and sleep; and the alternation between internal reflection and external attention. Bifurcation analysis of the brain-inspired model BCWNMM constructed in this study indicates that state transitions between steady and non-steady states at different bifurcation points may correspond to the brain's state transition mechanisms.

The neurodynamic characteristics of NMM gradually become monotonous when parameters exceed a specific range. Multiple limit cycle oscillation ranges can be generated when the parameters of the BCWNMM are set within an appropriate range. In addition, a special asymmetric branch curve is generated at the branch point, causing asymmetry in the output between the two models. Since $P(t)$ follows a normally

distributed Gaussian white noise and the system input components are constantly changing, the output of BCWNMM may be affected by both symmetric bifurcation diagrams and asymmetric bifurcation diagrams. The limit cycle at point H_3 in Fig. 3 can generate various types of signal outputs (*e.g.*, spike-shaped, theta wave-shaped, *etc.*). Therefore, multi-channel coupled NMM has more complex dynamic characteristics compared with the single-channel model. In addition, each bifurcation diagram of the BCWNMM corresponds to multiple stable parameter intervals, exhibiting a variety of nonlinear dynamic characteristics.

We found that the BCWNMM can generate epileptic-like EEG signals by simply changing the coupling strength C. This indicates that they can generate more complex nonlinear dynamic characteristics when NMMs are coupled together, thereby producing EEG-like signals with complex dynamic characteristics. The reception region is affected by different bifurcation curves when the emission region changes in the bistable interval. This reflects the interaction and mutual influence between two mutually coupled NMMs. The unidirectional coupling output exhibits a bifurcation phenomenon because the NMM of the emission region exhibits a multi-stable phenomenon. Furthermore, only one bifurcation is active at a time; two cannot occur simultaneously. The cause of branching in the BCWNMM is due to branching points.

Although the BCWNMM constructed in this study successfully reveals synchronous and asynchronous dynamic behaviors emerging with variations in coupling strength, it must be noted that this work still has certain limitations. These limitations also point the way forward for future research. On the one hand, this study makes an idealized assumption regarding information transmission delays, namely that information exchange between the two models occurs instantaneously. However, the presence of physical pathways inevitably leads to signal transmission delays in actual functional brain networks. Time delays may alter the dynamic properties of coupled systems, induce complex neural oscillation patterns, and even cause models to exhibit chaotic behavior. Discussion of time delays is beyond the scope of this study. On the other hand, this study has limitations in terms of scale and diversity. The current research is limited to coupling between two identical Wendling models, which represents only a highly simplified abstraction of the brain's complex networks. To construct mathematical models that more closely approximate physiological processes, future research should expand the number of network nodes and investigate the collective dynamics of large-scale Wendling model clusters. Furthermore, future research will integrate hippocampal, thalamic, and visual models to explore the complex dynamic interactions between different functional regions of the brain.

5. Conclusion

The present study utilizes bifurcation analysis to investigate the nonlinear dynamical properties of the BCWNMM and analyzes the bifurcation phenomena produced by the system when the coupling strength changes. In bidirectional coupling experiments, there are multiple bifurcation diagrams in the system, and multiple bifurcation curves exist simultaneously and affect the model's output. Moreover, the system can simulate epileptic-like brain signals for symmetric bifurcation diagrams by changing the coupling strength. The receiving channel is affected by multiple bifurcation curves in a unidirectional coupling experiment. However, multiple bifurcation curves do not simultaneously affect the model output. In addition, regardless of the coupling method used, characteristics such as bifurcation points and limit cycles only exist within a narrow range of parameters. The dynamic characteristics of the model become monotonous when the parameter values are too small or too large. Consequently, BCWNMM coupled models exhibit more intricate dynamic characteristics in comparison to a single-region Wendling model and can be utilized as a means of analyzing the coupling relationship between any two brain regions.

Appendix A: Parameters used in models

Table 1. Standard values and physiological interpretations of the parameters in models.

Paras	Interpretation	Standard value
A	Average excitatory synaptic gain	3.25
B	Average inhibitory synaptic gain	22
G	Average fast inhibitory synaptic gain	9 mV
a	Average excitatory time constant	100 s^{-1}
b	Average inhibitory time constant	25 s^{-1}
g	Reciprocal of average fast inhibitory time constant	500 s^{-1}
C_1, C_2	Average number of synaptic contacts in the excitatory feedback loop	$C_1 = 135$, $C_2 = 0.8C_1$
C_3, C_4,C_5, C_6, C_7	Average number of synaptic contacts in the slow feedback inhibitory loop Average number of synaptic contacts in the fast feedback inhibitory loop	$C_3 = C_4 = 0.25C_1$, $C_5 = 0.3C_1$, $C_6 = 0.1C_1$, $C_7 = 0.3C_1$
v_0, e_0, r	Parameters of nonlinear sigmoid function Sigmoid	$v_0 = 6$ mV, $e_0 = 2.5$ s^{-1}, $r = 0.56$ mV
u, σ^2	The mean and variance of the external input	$u = 90$, $\sigma^2 = 30$

Acknowledgements

Project supported by the National Natural Science Foundation of China (Grant Nos. 62173291 and 62303396) and the Natural Science Foundation of Hebei Province, China (Grant Nos. F2024203049 and H2024203007).

References

[1] Alexander D M, Trengove C and van Leeuwen C 2015 *Cogn Process* **16** 365
[2] Grieder M, Koenig T, Kinoshita T, Utsunomiya K, Wahlund L O, Dierks T and Nishida K 2016 *Clinical Neurophysiology* **127** 2175
[3] Liu J, Zhang P, Zou Q, Liang J, Chen Y, Cai Y, Li S, Li J, Su J and Li Q 2023 *Epilepsia Open* **8** 32
[4] Zhao C, Huang W- J, Feng F, Zhou B, Yao H X, Guo Y E, Wang P, Wang L N, Shu N and Zhang X 2022 *Neural Regeneration Research* **17** 2014
[5] Coronel-Oliveros C, Gómez R G, Ranasinghe K, Sainz-Ballesteros A, Legaz A, Fittipaldi S, Cruzat J, Herzog R, Yener G, Parra M, Aguillon D, Lopera F, Santamaria-Garcia H, Moguilner S, Medel V, Orio P, Whelan R, Tagliazucchi E, Prado P and Ibañez A 2024 *Alzheimer's & Dementia* **20** 3228
[6] Kirillov S Y, Zlobin A and Klinshov V V 2023 *Izvestiya VUZ. Applied Nonlinear Dynamics* **31** 757
[7] Wilson H R and Cowan J D 1972 *Biophysical Journal* **12** 1
[8] Freeman W J 1972 *Annual Review of Biophysics* **1** 225
[9] Lopes da Silva F H, Hoeks A, Smits H and Zetterberg L H 1974 *Kybernetik* **15** 27
[10] Jansen B H and Rit V G 1995 *Biol. Cybern.* **73** 357
[11] Wendling F, Bartolomei F, Bellanger J J and Chauvel P 2002 *European Journal of Neuroscience* **15** 1499
[12] David O, Cosmelli D and Friston K J 2004 *NeuroImage* **21** 659
[13] Cui D, Li X, Ji X and Liu L 2011 *Sci. China- Inf. Sci.* **54** 1283
[14] Haan W de, Straaten E C W van, Gouw A A and Stam C J 2017 *PLOS Comput. Biology* **13** e1005707
[15] Honey C J, Sporns O, Cammoun L, Gigandet X, Thiran J P, Meuli R and Hagmann P 2009 *Proc. Natl. Acad. Sci. USA* **106** 2035
[16] Breakspear M R, Terry J and Friston K J 2003 *Neurocomputing* **52–54** 151
[17] Larter R, Speelman B and Worth R M 1999 *Chaos* **9** 795
[18] Cakan C, Jajcay N and Obermayer K 2023 *Cogn. Comput.* **15** 1132
[19] Cooray G K, Rosch R E and Friston K J 2023 *PLOS Comput. Biology* **19** e1010915
[20] Zarei Eskikand P, Soto-Breceda A, Cook M J, Burkitt A N and Grayden D B 2023 *Neural Networks* **166** 296
[21] Spiegler A, Kiebel S J, Atay F M and Knösche T R 2010 *NeuroImage* **52** 1041
[22] Huang G, Zhang D, Meng J and Zhu X 2011 *Neurocomputing* **74** 1026
[23] Xin-lei A and Li Z 2018 *Nonlinear Dyn.* **94** 2995
[24] Sen Bhattacharya B, Cakir Y, Serap-Sengor N, Maguire L and Coyle D 2013 *Neurocomputing* **115** 11
[25] Ahmadizadeh S, Karoly P J, Nešić D, Grayden D B, Cook M J, Soudry D and Freestone D R 2018 *PLOS One* **13** e0192842
[26] Clusella P, Deco G, Kringelbach M L, Ruffini G and Garcia-Ojalvo J 2023 *PLOS Comput. Biology* **19** e1010781
[27] Shao H, Gu G, Guo X, Li X and Cui D 2025 *Computer Methods and Programs in Biomedicine* **263** 108675
[28] Cui D, Li H, Shao H, Gu G, Guo X and Li X 2024 *Brain Sciences* **14** 240
[29] Cui D, Li H, Liu P, Gu G, Li X, Wang L and Yin S 2022 *J. Neural Eng.* **19** 066043
[30] Petkoski S and Jirsa V K 2019 *Phil. Tran. Roy. Soc. A: Math. Phys. Eng. Sci.* **377** 20180132
[31] Jiang L, Li F, Chen Z, Zhu B, Yi C, Li Y, Zhang T, Peng Y, Si Y, Cao Z, Chen A, Yao D, Chen X and Xu P 2023 *NeuroImage* **270** 119997
[32] Wang Z, Dai Z, Gong G, Zhou C and He Y 2015 *Neuroscientist* **21** 290
[33] Banks M I, White J A and Pearce R A 2000 *Neuron* **25** 449
[34] Schirner M, McIntosh A R, Jirsa V, Deco G and Ritter P 2018 *eLife* **7** e28927
[35] Swami P, Panigrahi B K, Nara S, Bhatia M and Gandhi T 2016 *EEG Epilepsy Datasets*
[36] Grimbert F and Faugeras O 2006 *Neural Computation* **18** 3052
[37] Geng S and Zhou W 2016 *J. Integr. Neurosci.* **15** 463
[38] Wang X J, Gu H G, Jia Y B, Lu B and Zhou H 2023 *Chin. Phys. B* **32** 090502
[39] Ma L, Ren Y L, He A J, Cheng D Q and Yang X D 2023 *Chin. Phys. B* **32** 110506
[40] Ramantani G, Westover M B, Gliske S, Sarnthein J, Sarma S, Wang Y, Baud M O, Stacey W C and Conrad E C 2023 *Epilepsia* **64** S25